Separate measurements of magnetic and pressure thrust contributions in a magnetic nozzle electron cyclotron resonance plasma thruster

Théo Vialis, Julien Jarrige, Denis Packan

Separate measurements of magnetic and pressure thrust contributions in a magnetic nozzle electron cyclotron resonance plasma thruster

SPACE PROPULSION 2018
BARCELO RENACIMIENTO HOTEL, SEVILLE, SPAIN / 14 – 18 MAY 2018

Théo Vialis[(1)], Julien Jarrige[(2)] and Denis Packan[(3)]
[(1)]ONERA-The French Aerospace Lab, 91120 Palaiseau, France, email: theo.vialis@onera.fr
[(2)]ONERA-The French Aerospace Lab, 91120 Palaiseau, France, email: julien.jarrige@onera.fr
[(3)]ONERA-The French Aerospace Lab, 91120 Palaiseau, France, email: denis.packan@onera.fr

KEYWORDS: Electric propulsion, magnetized plasmas, magnetic nozzle, electron cyclotron resonance

ABSTRACT: A recurring question in magnetic nozzle plasma thrusters is the origin of the thrust which is a combination of plasma expansion (driven by the electron pressure) and diamagnetic effects in the divergent magnetic field. In this paper, direct thrust measurements are performed separately on the plasma source and on the permanent magnet of ONERA Electron Cyclotron Resonance plasma thruster. This allows for a quantification of the respective contributions of the electron pressure thrust that acts on the plasma source and the magnetic thrust that acts on the magnet. It has been found that the ratio of magnetic thrust to total thrust (T_B/T_{tot}) is constant around 70% when the thruster is operated with a xenon mass-flow rate of 0.1 mg/s and a power in the range 20-60 W range. On the other hand, the contribution of magnetic thrust strongly depends on the mass flowrate: the ratio T_B/T_{tot} decreases from 80% to 55% when the flowrate is increased from 0.06 to 0.25 mg/s (with 40 W of injected power).

1. INTRODUCTION

The reduction of the take-off weight of satellites motivates the research on alternatives technologies to chemical space thrusters such as electric (or plasma) thrusters. Electric thrusters have a better propellant mass utilization than chemical thrusters, thus reducing the mass of onboard propellant for equivalent missions or extending mission lifetime. However, the produced thrust is low compared to chemical thrusters.

In electric propulsion the thrust is produced by the ejection of ions that are created and accelerated by different electromagnetic processes depending on the thruster technology. The most common technologies of electric propulsion are: Gridded Ion Engines (GIE) and Hall Effect Thrusters (HET). These technologies also have some drawbacks, in particular a neutralization cathode is required, which is a critical component. Possible alternatives to ion thrusters are electrodeless plasma thrusters that are currently being developed like the Helicon plasma thruster (HPT) [1], the Electron Cyclotron Resonance plasma thruster (ECR) [2] and the VASIM-R project [3]. These three technologies combine plasma-wave absorption with a static magnetic field to produce and drive the plasma to the exhaust where the plasma is expanding in a divergent magnetic field (the magnetic nozzle). The usable momentum gain provided by the expanding plasma in the magnetic nozzle thrusters is still an active research topic because the physics is not fully understood yet. The mechanisms that accelerate the ions in this expanding zone could be thermal or magnetic. Different models (fluid, kinetic and hybrid) have been built to study the physics in the magnetic nozzle (MN), which is essential for the understanding of the ion acceleration and for the plasma detachment [4].

Direct thrust measurements have shown that with a strong enough magnetic field, the magnetic thrust could be preponderant over electron pressure thrust [5]. These experiments have been performed on a 100-600 W HPT and results have been compared to a fluid model [6, 7].

In this paper, direct thrust measurements are performed on an Electron Cyclotron Resonance (ECR) plasma thruster. The section 2 will present the set-up and the measurement methods while section 3 will show the results.
This study aims at assessing the importance of magnetic thrust and electron pressure thrust in a magnetic nozzle plasma thruster, and also at quantifying the proportion of magnetic thrust over the total thrust as a function of microwave power and xenon mass flowrate.

2. EXPERIMENTAL SET-UP

The electron-driven magnetic nozzle plasma thruster used in this study is the Electron Cyclotron Resonance (ECR) plasma thruster developed at ONERA since 2010. It consists of a semi-open coaxial cavity immersed into a static magnetic field created by a 70 mm outer diameter and 26 mm inner diameter annular Nd-Fe-B magnet. The plasma is created in a 20 mm long and 27.5 mm diameter cylinder called the “plasma source” by the resonance of the electrons with the incoming electromagnetic wave. This resonance takes place locally, close to the backwall of the source. It happens when the cyclotron frequency of the electron is close to the frequency of the wave, which is 2.45 GHz (corresponding to a resonant magnetic field magnitude of 875 G) in this model. The power of the microwave is then efficiently transferred to the electrons, which generates and maintains a plasma in the source. The plasma is accelerated at the open exit by two main processes: plasma expansion (driven by the electron pressure) and diamagnetic effects in the divergent magnetic field. The difference of mobility between the ions and the electrons creates an ambipolar electric field that maintains the quasi-neutrality of the current-free plasma beam and accelerates the ions. The thruster is electrically isolated from the facility ground with a DC-Block for insuring the current-free aspect of the plasma beam.

In this configuration, the thruster is operated with microwave input power in the range 20-60 W, and with xenon mass-flow rate in the range 0.05-0.25 mg/s. The thrust range is from 300 µN to 1.2 mN. Previous works on this model have shown that the specific impulse can be as high as 1200 s and the total efficiency can reach 12.5 % [8].

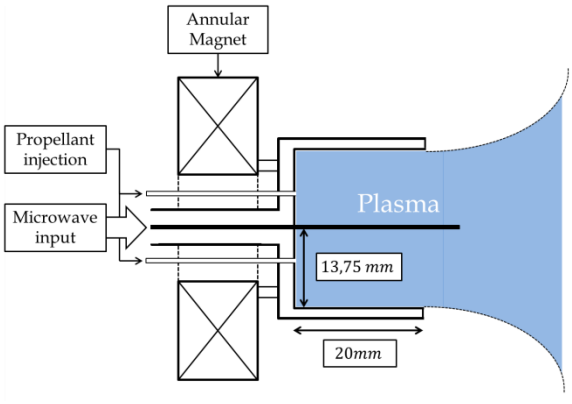

Figure 1. Schematic of the ECR plasma thruster (not in scale)

The measurements presented in this paper are performed in the 4 m long and 1 m diameter cylindrical vacuum chamber (B61 facility at ONERA Palaiseau). The pumping system consists of a turbo-molecular pump and a cryogenic pump for a total pumping speed of 8000 l/s for xenon. The xenon mass-flow rate (Q_m) is injected using a mass-flow controller with a 1 mg/s full scale. The microwave power is measured on the microwave line with a dual coupler and diodes. Forward and reflected power are then combined together taking in account the attenuation of the line between the coupler and the thruster in order to have the power, *P*, transmitted to the thruster. *P* is then the power used for all the results shown in this paper and it is measured with a 4% uncertainty.

The thrust value is obtained by two methods: directly via a pendulum thrust balance [9, 10] and indirectly with ion current and ion energy measurements.
The thrust balance is regulated by a PID control system. The PID maintains the arm of the balance at the equilibrium position. When the thruster is operated, the thrust is balanced by a force applied by an actuator (planar coil acting on magnets). The displacement of the balance arm is measured with a capacitive sensor, while the current in the actuator is controlled by the PID control system. The current sent to the actuator is proportional to the thrust.
Figure 2 shows a typical direct thrust measurement obtained with thrust balance. Firstly, the thruster is

ignited. After a few seconds, the operation conditions (P and Q_m) are set. When steady-state is reached, the power is suddenly turned off, producing a step of signal whose amplitude is proportional to the step of thrust.
The proportionality coefficient is deduced from an absolute calibration.

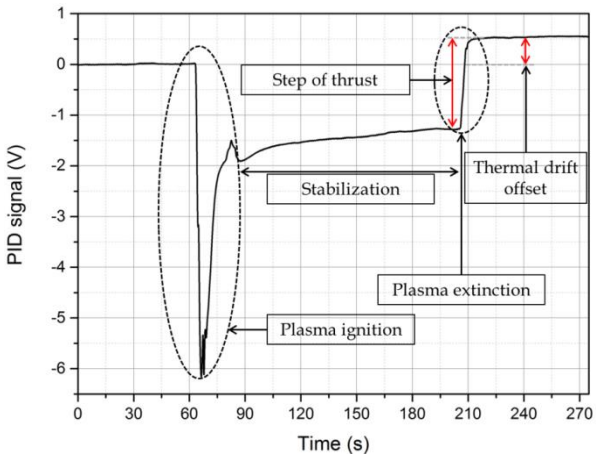

Figure 2. Typical thrust signal during a thrust measurement acquisition

The calibration is performed by the deposition of small masses, with a known weight, on a calibration arm. The recorded signal is compared to the torque created by the masses in order to obtain the calibration factor. A set of five calibrated masses are deposited in order to cover a thrust range from 100 µN to 1.5 mN.

The thrust T can also be estimated from the angular profile of the ion current density J_i and from the mean ion total energy E_i in the axis [11, 12]. Both measurements are performed with a gridded Faraday probe mounted on a rotation stage. The thrust is given by the following expression:

$$T = \int_{-90}^{90} \frac{M_i}{e} J_i(\varphi)\, 2\pi D^2 \sqrt{2E_i/M_i}\, \sin(\varphi)\cos(\varphi)\, d\varphi$$

where M_i and e are respectively the ion mass and the elementary charge, D is the distance between the probe and the thruster, and φ is the angle of rotation of the probe (with respect to the thruster axis). J_i is measured in the ionic saturation region, i.e. by applying a constant negative bias on the Faraday probe's collector. E_i is obtained by performing an energy scan with the gridded Faraday probe [13].

A suitable experimental thrust balance set-up is used to directly measure the two contributions of the thrust: electron pressure and magnetic nozzle. Indeed, the two contributions of the entire force are not applied on the same part of the thruster: electron pressure (thermal thrust) acts directly on the plasma source backwall while the diamagnetic effect (magnetic thrust) acts on the magnet. Furthermore, the plasma source and the permanent magnet of this thruster prototype can be physically separated. Instead of fixing the whole thruster on the balance arm, one can fix only the source or the magnet on the balance arm in order to measure its respective contribution (*Figure 3*).

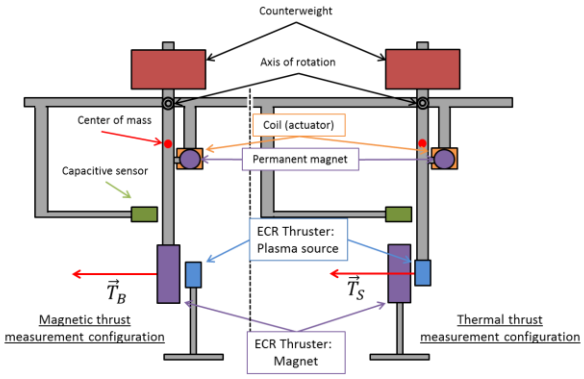

Figure 3. Schematic of the thrust balance adapted for the separate measurement of the thrust components

3. MEASUREMENTS

An experimental campaign has been led to measure the two contributions of thrust. Thrust measurements have been performed in three steps: first standard measurement (source + magnet, T_{tot}), then measurement on the source (T_S) alone, and finally measurement on the permanent magnet alone (T_B). In order to verify that the thruster had the same behavior during the three experiments, the performances estimated with the Faraday probe are compared in the same conditions (*Figure 4*).

The uncertainties on the direct thrust measurement are represented as errors bars on the figures. They

are computed using standard error propagation. The total thrust uncertainty is estimated between 2% and 4% in the 500-1000 µN range (See [10] for the more detailed expression). Errors over the indirect (Faraday probe) measurements are not calculated here because it is difficult to assess the different terms for ion current (sheath expansion, secondary electron emission, etc…).

Figure 4 shows the thrust inferred from the probe measurements with respect to the power for a mass flow rate of 0.1 mg/s of xenon. The thrust is estimated for the three experimental configurations.

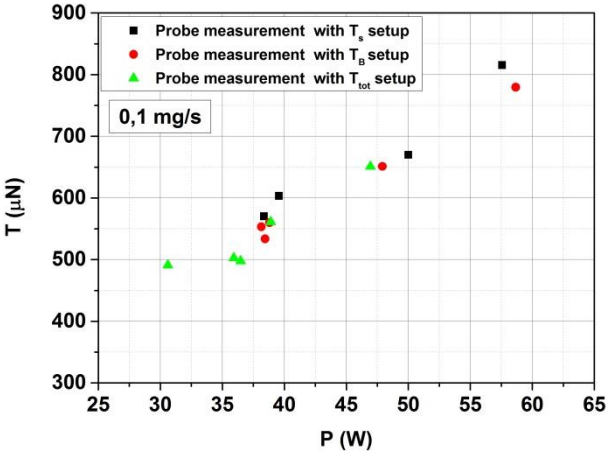

Figure 4. Thrust inferred from probe measurements as a function of injected power for a constant mass-flow rate. The three datasets correspond to the three balance measurement setups

These results confirm that the three experiments have been conducted in the same conditions because the Faraday probe measurements give approximately the same thrust level for equivalent operation conditions. This enables to compare the direct thrust measurements on the different parts of the thruster.

These results are particularly relevant, knowing that this setup adds an uncertainty over the position of the resonant zone in the plasma source. It is noteworthy that the direct measurements of the total thrust and the thrust value inferred from probe measurements are not exactly the same (mainly because of the uncertainty on ion current). However, similar trends are obtained for both diagnostics.

Figure 5 (top) presents the results obtained with the thrust balance for the three different cases as a function of *P* (the injected power). In every case, the thrust increases with the power. The sum of the thrust on the source (T_S) and the thrust on the magnet (T_B) is compared to the total thrust (source and magnet together) on the *Figure 5*. Thrust values are very close at low power (20-30 W); however for higher power, the sum of T_S and T_B tends to be higher than T_{tot} (the deviation reaches 15% at 60 W).

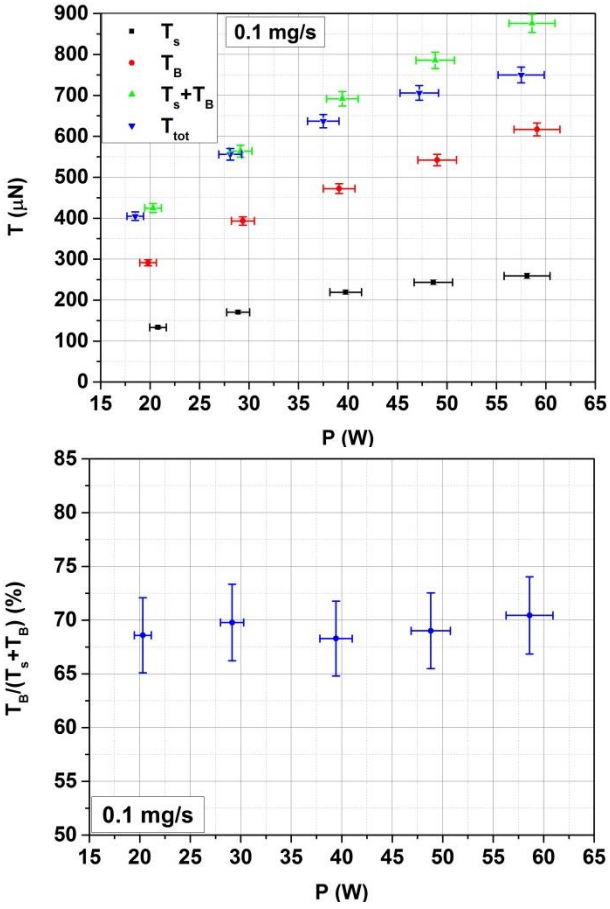

Figure 5. Top: direct measurement of the thrust applied on the source T_S, on the magnet T_B, $T_S + T_B$, and total measured thrust T_{tot} versus injected power. Bottom: ratio of magnetic thrust T_B to the sum T_s+T_B versus the injected power. Q_m=0.1 mg/s

Between 20 W and 60 W, the thermal thrust (T_S) increases from ~130 µN to ~280 µN while the magnetic thrust goes from ~300 µN to ~600 µN. The magnetic thrust dominates in this case and it represents approximatively 70% of the total thrust (*Figure 5* bottom). It is noteworthy that this ratio is constant in the whole power range tested here.

Figure 6 (top) shows the different measured thrusts when the mass-flow rate is changed in the range 0.06-0.25 mg/s while the injected power is kept constant at 40 W. The measured total thrust T_{tot} and the sum of the magnetic (T_B) and thermal (T_S) thrust are in agreement for low mass flowrate (<0.125 mg/s), while a slight difference (up to 12%) can be noticed for high mass-flow rate. Thermal thrust monotonically increase with Q_m from ~130 µN to 380 µN, whereas magnetic thrust slightly increases from 0.06 mg/s to 0.125 mg/s (with a maximum T_B around 550 µN), and tends to decrease for higher mass flowrates. The relative variations of T_B are not higher than 10% in this mass-flow rate range. Because of this particular behavior, the fraction of the magnetic thrust decreases from 77% at 0.06 mg/s to almost 56% at 0.25 mg/s.

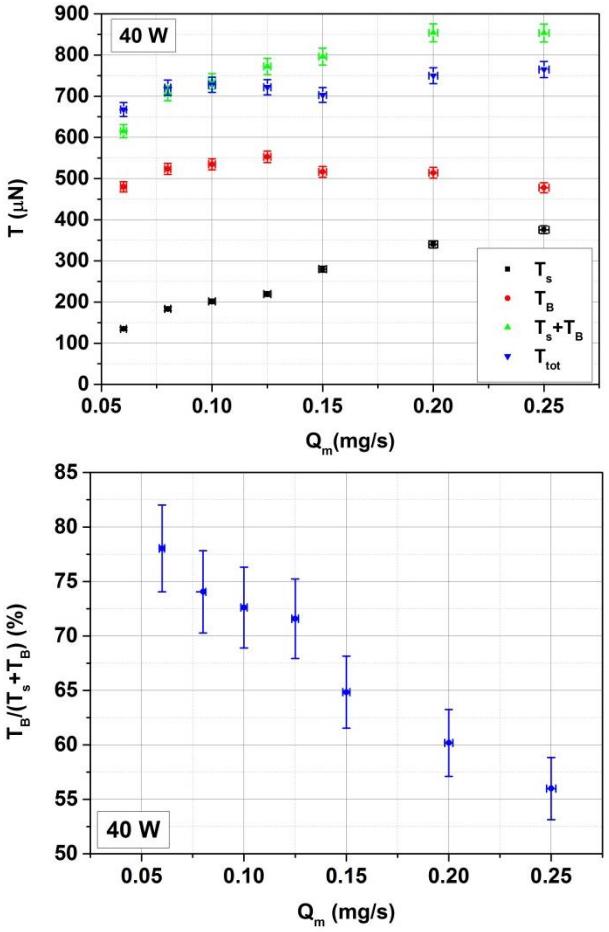

Figure 6. Top: direct measurement of the thrust applied on the source T_S, on the magnet T_B, T_S+T_B, and total measured thrust T_{tot} versus xenon mass-flow rate. Bottom: ratio of the magnetic thrust T_B to the sum T_S+T_B versus the xenon mass-flow rate. P= 40 W.

4. DISCUSSION

In order to interpret these results, the following theoretical expression of the total axial thrust (in cylindrical coordinates) is used [5, 6]:

$$T_{tot} = \underbrace{2\pi \int_0^{r_p(z)} r\, p_{e\parallel} dr}_{T_S} - \underbrace{2\pi \int_{z_0}^{z}\int_0^{r_p(z)} r \frac{B_r}{B_z} \frac{\partial p_{e\perp}}{\partial r} dr dz}_{T_B} \quad (1)$$

Where $p_e = n\, k_B\, T_e$ is the electron pressure, n the plasma density, T_e the electron temperature, $r_p(z)$ the plasma radius (i.e. radius of the plume), B_r and B_z respectively the radial and axial component of the magnetic field. The subscripts ∥and ⊥ refers to the parallel and perpendicular contributions of p_e or T_e with respect to the magnetic field vector field.

The first term in eq. (1) corresponds to the thrust applied on the plasma source (T_S) and the second one is the magnetic thrust (T_B) applied on the magnet. This formula comes from fluid equations (for electrons and ions) in the plume assuming an axisymmetric, collision-less, quasi-neutral and steady-state plasma, and neglecting cold gas momentum, electron inertia and ion pressure.

This section is focused on the understanding of the evolution of the two different components of the thrust with variation of the power and the mass-flow rate. According to eq.(1), variations of T_B and T_S when changing P and Q_m are only due to variations of the radial profile of electron perpendicular and parallel pressures. Indeed, the other quantities (B_r/B_z, $r_p(z)$) of eq. (1) are supposed to be constant with respect to the operating conditions.

It is known that the electron temperature (parallel or perpendicular) and the plasma density (up to a certain point) increase with respect to the injected power [2, 12]. So, the electron pressure, in particular its parallel component, increases with power. This explains the monotonic increase of T_S on Figure 5 (top).

Using paraxial approximation, one can simplify T_B as [6, 7]:

$$T_{B,p} = \int_0^z \langle p_{e\perp} \rangle A(z) \frac{1}{B_z} \frac{\partial B_z}{\partial z}\, dz \quad (2)$$

where $\langle p_{e\perp} \rangle$ is the radially averaged perpendicular electron pressure and $A(z) = 2\pi r_p(z)$ is the plasma area (for a given longitudinal position z in the plume). The only term that is affected by the power level in equation (2) is $\langle p_{e\perp} \rangle$. Therefore the observed increase of T_B with power on Figure 5 (top) means that the perpendicular electron pressure is globally increased. This result is in line with previous characterization of the ECR thruster performed with a diamagnetic loop, which has shown that the perpendicular electron pressure (measured in the source) increases with injected power [14].

When increasing the mass-flow-rate for a constant injected power in a plasma, the density is generally increased while the electron temperature is decreased [2, 12]. This is due to an increase of the collision frequency of the electrons with neutrals, which could lead to an isotropization of the electron temperature (and then of the electron pressure). Indeed, in the ECR thruster, the electrons are heated by the resonance process that increases their perpendicular temperature, while their parallel temperature is only increased through collisions and diamagnetic effect [15].
In eq. (1) the T_S expression only involves the parallel component of the pressure which is supposed to increase with the isotropization and then with Q_m. This could explain why T_S is monotonically increasing on Figure 6 (top).
On the other hand, diamagnetic loop measurements have shown that the perpendicular electron pressure is almost constant with respect to the mass-flow rate, as a result of the competition density increase and electron temperature drop [14].This observation and eq. (2) could explain the low variations of T_B with respect to the xenon mass-flow rate on Figure 6 (top).

5. CONCLUSION

An experimental campaign on a thrust balance has been led to measure separately the magnetic thrust and the electron pressure thrust of the ONERA ECR plasma thruster. The repeatability of the thruster has been verified for the three configurations (plasma source alone, magnet alone, and whole thruster on the balance) using Faraday probe measurements.

The magnetic thrust represents 70% of the total thrust when the thruster is operated at 0.1 mg/s of xenon mass-flow rate and with injected electric power between 20 and 60 W. By varying the xenon mass-flow rate, it has been shown that the fraction of magnetic thrust component decreases from 80% to 55% when the mass-flow rate is increased from 0.06 mg/s to 0.2 mg/s (with a constant injected power of 40 W).
Future works will include the use of a full 3D PIC (particle in cell) code, which is currently developed at ONERA, in order to analyze the different thrust contributions as a function of the operation parameters.

REFERENCES:

1. R.W. Boswell, “Very Efficient Plasma Generation By Whistler Waves Near The Lower Hybrid Frequency”, *Plasma Phys. and Controlled Fusion*, Vol.**26**, No10, pp. 1147 1162, (1984)
2. Cannat, F., Lafleur, T., Jarrige, J., Chabert, P., Elias, P-Q. and Packan, D., “Optimization of a Coaxial Electron Cyclotron Resonance Plasma Thruster with an Analytical Model”, Phys. Plasmas, Vol.**22**, No.5, pp. 053503, (2015)
3. Longmier B.W. et al., “VX-200 Magnetoplasma Thruster performance results exceeding fifty-percent Thruster efficiency”, Technical Notes in Journal Propulsion Power, Vol.**27**, No. 4, July-August, 2011
4. Ahedo, E., Merino, M., “Two-dimensional Supersonic Plasma Acceleration in a Magnetic Nozzle”, *Phys. Plasmas*, **17**, 073501, (2010)
5. Takahashi, K., Lafleur, T., Charles, C., Alexander, P., Boswell R.W., “Electron Diamagnetic Effect on Axial Force in an Expanding Plasma: Experiment and Theory”, *Phys. Rev. Lett.,***107**, 235001, (2011)
6. Fruchtman, A., Takahashi, K., Charles, C. and Boswell, R.W., “A Magnetic Nozzle Calculation of the Force on a Plasma”, *Phys. Plasmas*, **19**, 033507, (2012)
7. Takahashi, K., Charles, C., Boswell R.W., “Approaching the Theoretical Limit of Diamagnetic-Induced Momentum in a Rapidly Diverging Magnetic Nozzle” *Phys. Rev. Lett.,***110**, 195003, (2013)
8. Vialis, T., Jarrige, J., Packan, D., “Geometry Optimization and Effect of Gas Propellant in an Electron Cyclotron Resonance Plasma

Thruster", International Electric Propulsion Conference, Paper IEPC-2017-378, (2017)
9. Jarrige, J., Thobois, P., Blanchard, C., Elias, P-Q., Packan, D., Fellerini, L. and Noci, G., "Thrust Measurements of the Gaia Mission Flight-Model Cold Gas Thruster", *J. of Propul. Power*, Vol. **30**, No. 4, pp. 934-943, (2014)
10. Vialis T., Jarrige J., Packan D., Aanesland A, "Direct Thrust Measurement of an Electron Cyclotron Resonance Plasma Thruster", submitted to *J. of Propul. Power*, 2018
11. Jarrige, J., Elias, P-Q., Cannat, F. and Packan, D., "Characterization of a coaxial ECR plasma thruster", AIAA, Paper No. 2013-2628, 2013
12. Lafleur T., Cannat F., Jarrige J., Elias P-Q. and Packan D., "Electron dynamics and ion acceleration in expanding-plasma thrusters", *Plasma Sources Sci. Technol.*, Vol.**24**, 065013, 2015
13. Lafleur T., "Helicon plasma thruster discharge model", Phys. Plasmas, Vol.**21**, 043507, 2014
14. Correyero S., Jarrige, J., Packan. D., Ahedo. E., "Measurement of anisotropic plasma properties along the magnetic nozzle expansion of an Electron Cyclotron Resonance Thruster", Paper IEPC-2017-437, October 2017.
15. Geller, R., "Electron Cyclotron Resonance Ion Sources and ECR Plasmas", Institute of Physics Publishing Bristol and Philadelphia, ISBN 0750301074, 1996